Geophysical Research Letters

RESEARCH LETTER
10.1029/2023GL103545

Synergetic Effects of Isoprene and HO_x on Biogenic New Particle Formation

Lee Tiszenkel[1] and Shan-Hu Lee[1,2]

[1]Department of Atmospheric and Earth Sciences, University of Alabama in Huntsville, Huntsville, AL, USA, [2]Department of Chemistry, University of Alabama in Huntsville, Huntsville, AL, USA

Key Points:

- Isoprene can suppress or enhance biogenic new particle formation (NPF) depending on the oxidation regime (OH vs. ozone oxidation)
- Biogenic NPF is affected by both biogenic volatile organic compounds (VOCs) composition and HO_x conditions
- Previous laboratory studies showed seemingly contradicting theories because of the vastly different VOCs and HO_x conditions

Supporting Information:

Supporting Information may be found in the online version of this article.

Correspondence to:

S.-H. Lee,
shanhu.lee@uah.edu

Citation:

Tiszenkel, L., & Lee, S.-H. (2023). Synergetic effects of isoprene and HO_x on biogenic new particle formation. *Geophysical Research Letters*, *50*, e2023GL103545. https://doi.org/10.1029/2023GL103545

Received 7 MAR 2023
Accepted 25 JUN 2023

Abstract New particle formation (NPF) has been observed at various locations, but NPF does not occur in isoprene-dominant forests. Recent laboratory studies were conducted to understand the role of isoprene in biogenic NPF, and these studies show that isoprene can suppress biogenic NPF, with contradicting theories. To reconcile these discrepancies, we conducted flow tube experiments of biogenic nucleation under a wide range of isoprene over monoterpene carbon ratios (R) and oxidant conditions (OH vs. ozone). Our results show isoprene either suppresses or enhances biogenic NPF, depending on R and oxidation regimes, demonstrating the synergetic effects of isoprene and HO_x (OH and HO_2) on biogenic NPF. Whereas the suppression of NPF by isoprene is due to the product suppression effects of monoterpene dimers (C20), $RO_2 + HO_2$ termination reactions also play important roles in suppressing the dimer formation, another likely process to suppress NPF in the atmosphere.

Plain Language Summary Isoprene, emitted mainly from broad-leaf trees, is the most important volatile organic compound at the global scale. Yet, the role of isoprene in new particle formation (NPF) is still unclear and studies often show contradicting results. In this study, using the state-of-the art mass spectrometer analysis, we show how oxidation reactions of isoprene can suppress or enhance biogenic NPF under different oxidation conditions. We believe our results help to reconcile the discrepancies that exist in the previous biogenic NPF studies.

1. Introduction

New particle formation (NPF) is the main source of secondary aerosols in the atmosphere. Observations show NPF can enhance CCN concentrations by a factor of 0.5–11 at the regional scale (S.-H. Lee et al., 2019). Global modeling simulations also show NPF can contribute up to 70% of the global CCN (Gordon et al., 2017). NPF events have been observed at various locations and occur most frequently in the free troposphere and lower stratosphere, extremely polluted Chinese mega-cities, and boreal forests (Kerminen et al., 2018; S.-H. Lee et al., 2019). However, NPF occurs extremely rarely in forests with dominant isoprene emissions (Kanawade et al., 2011; S.-H. Lee et al., 2016, 2019). Long-term, continuous aerosol measurements have been made in Amazon rainforests over the last decades and these measurements show that NPF does not occur, either at the forest sites (Pöhlker et al., 2012) or the sites influenced by biomass burning emissions (Rissler et al., 2006). There are so far eight different mixed forests in the United States where aerosol size distributions have been made: for example, in upper Michigan (Kanawade et al., 2011), Whiteface Mountain (Bae et al., 2010), Pinnacle State Park (Bae et al., 2010), Duke forests (Pillai et al., 2013), a rural Alabama forest (S.-H. Lee et al., 2016), and a high-elevation mountaintop site in Steamboat Spring in Colorado where temperatures are low (around 5°C, a very favorable condition for aerosol nucleation) (Hallar et al., 2015; F. Yu et al., 2015). All these sites showed that NPF rarely takes place during the summer with strong emissions of isoprene despite low condensation sink conditions, and some cases even in the presence of sulfuric acid, ammonia, and amines (Kanawade et al., 2011; S.-H. Lee et al., 2016). Without considering the absence of NPF in isoprene-rich forests, global models can over-predict the CCN production and thus over-predict the aerosol and cloud cooling effects over isoprene-dominant regions (Gordon et al., 2017). This represents an important climate science issue, as isoprene accounts for majority of the global volatile organic compound (VOC) emissions (Guenther et al., 2006).

The plant chamber experiments by Kiendler-Scharr et al. (2009) for the first time showed that isoprene can suppress biogenic NPF. To understand the chemical mechanisms behind the biogenic NPF in isoprene-dominant forests, several laboratory studies were conducted in recent years (Heinritzi et al., 2020; McFiggans et al., 2019;

Wang et al., 2021). These studies in general show that isoprene can suppress pure biogenic NPF. And they also show that the suppression is in part due to "product suppression effects" of C20 highly oxygenated organic molecules (HOMs) by isoprene-produced HOMs (C5 or C15). HOMs form from autoxidation reactions of organic peroxy (RO_2) radicals via intramolecular hydrogen shift, a reaction so called "autoxidation" (Bianchi et al., 2019; Frege et al., 2018; Iyer et al., 2021; Simon et al., 2020; Tröstl et al., 2016; Zhao et al., 2018). The "product suppression" can be explained intuitively as the following: in a biogenic VOCs system mixed with monoterpene and isoprene emissions, the C20 dimer formation from monoterpene C10 RO_2 can be reduced due to the RO_2 cross-reactions between isoprene-formed C5 and monoterpene C10 RO_2 radicals. C20 HOMs have very low volatilities (even lower than those of C15) so they are much more favorable for nucleation or NPF.

While these laboratory studies agreed on the product suppression effects on biogenic NPF, they showed contradicting mechanisms between each other or contradicting atmospheric observations. McFiggans et al. (2019) showed that biogenic NPF is suppressed because of the reduced OH by isoprene, in addition to production suppression effects. The reduction of OH is likely in an enclosed system (especially without NO_x), but in real forests OH is not reduced as shown by a number of observations (Di Carlo et al., 2004; Hofzumahaus et al., 2009; Kanawade et al., 2011; Lelieveld et al., 2008; Martinez et al., 2010; Paulot et al., 2009; Peeters et al., 2009). OH is rather regenerated by isoprene in the atmosphere, for example, during the autoxidation of RO_2 radicals (Bates & Jacob, 2019; Bianchi et al., 2019) or during the decomposition of Criegee intermediate biradicals (Finlayson-Pitts & Pitts, 2000; Seinfeld & Pandis, 2016). In contrast to McFiggans et al. (2019), Heinritzi et al. (2020) showed that even in an enclosed system like in the CERN Cosmics Leaving Outdoor Droplets (CLOUD) chamber, a higher level of OH radicals suppresses biogenic NPF, by increasing C5 and C15 HOMs (to cause even stronger product effects). Wang et al. (2021) flow tube experiments showed that isoprene can suppress biogenic NPF in the presence of OH, but in the absence of OH (i.e., under oxidation by ozone alone), isoprene can enhance NPF unlike other studies (Heinritzi et al., 2020; McFiggans et al., 2019).

Here, we show laboratory experiments of biogenic NPF under a large range of R (the ratio of isoprene carbons over monoterpene carbons) and oxidation conditions (ozone vs. OH) to reconcile these seemingly inconsistent roles that isoprene plays in biogenic NPF in the current literature (Heinritzi et al., 2020; McFiggans et al., 2019; Wang et al., 2021). We show the biogenic NPF is highly sensitive to the experimental conditions, and the differences in the literature occurred mostly because their experimental conditions were relatively polarized in terms of R and oxidation conditions. We also show that while product suppression effects play an important role in the suppression of biogenic NPF by isoprene, the $HO_2 + RO_2$ reactions compete with the formation of dimer HOMs (C15 and C20), as occurring in the atmosphere, to suppress the biogenic NPF.

2. Methods

The biogenic NPF experiments were conducted in the Tandem Aerosol Nucleation and Growth Environment Tube (Tiszenkel et al., 2019) setup (Figure S1 in Supporting Information S1). This is a dual-flow tube system where nucleation and growth can take place in separate independent environments. In the current study, the conditions in the two flow tubes were kept the same. While chamber studies analyze batch samples over a certain reaction time (e.g., half-hour), flow tube studies look at the snapshot of air samples at a specific residence time (e.g., 150 s, in our case). Flow tubes are easy to control experimental conditions, clean the wall, and characterize the wall loss (e.g., in a cylindrical tube). The Supporting Information S1 includes the detailed experimental procedures. Typical experimental conditions used in our study are shown in Table S1 in Supporting Information S1. Briefly, experiments were conducted at room temperature and dry conditions (RH < 10%). In our experiments, OH was generated from ozonolysis of VOCs (hence dark OH source, as opposed to ozone photolysis). HOMs produced from the oxidation of BVOCs were measured with the high-resolution time-of-flight chemical ionization mass spectrometer (HrTOF-CIMS) using iodide as a reagent (B. H. Lee et al., 2014). Both gas- and aerosol-phase HOMs were detected simultaneously, by attaching a Filter Inlet for Gas and AEROsol (Lopez-Hilfiker et al., 2014) inlet to HrTOF-CIMS. Impurities of ammonia and amines were measured with a CIMS using protonated ethanol as an ionization reagent (You et al., 2014; H. Yu & Lee, 2012). Since we did not introduce SO_2 into the system, it was assumed that no sulfuric acid was produced. Particle number concentrations larger than 1 nm were measured with a particle size magnifier (PSM, Airmodus A10) (Vanhanen et al., 2011). And particle sizes between 1 and 4 nm were estimated using the PSM-measured particle number concentrations under different fluid flow rates and with an inversion program developed by (Lehtipalo et al., 2014). Particle sizes

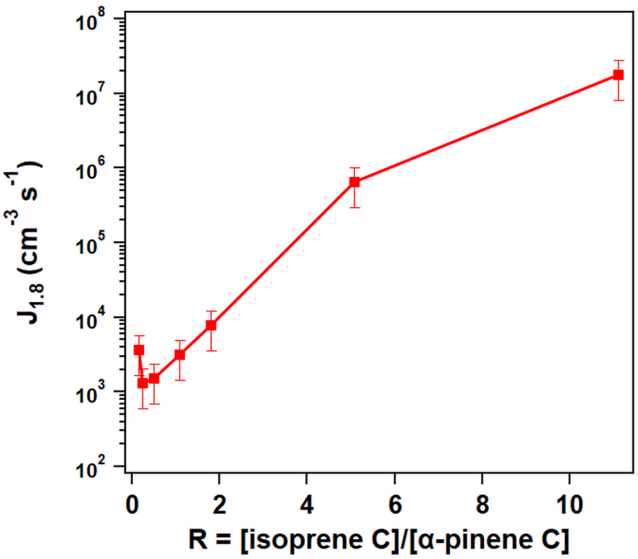

Figure 1. The measured nucleation rate $J_{1.8}$ as a function of R. Vertical bars indicate one standard variation in $J_{1.8}$. We have conducted the same experiments for 6 days, and these data showed the same trend as shown here. Data shown in this figure and Figures 2–4 are from the same day's experiments.

from 3 to 100 nm were measured with an scanning mobility particle sizer (TSI 3936N76) which consists of nano-differential mobility analyzer (TSI 3085) and butanol-based ultrafine condensation particle counter (TSI 3776).

3. Results and Discussions

Figure S2 in Supporting Information S1 shows the results taken from the pure α-pinene oxidation experiments at α-pinene of 60 ppb and ozone in the range from 0 to 3.2 ppm. The measured aerosol size distributions show increased particle number concentrations of sub-3 nm particles as well as ultrafine particles, with increasing HOM formation. The derived $J_{1.8}$ shows a power dependence of 4–5 with the P_{HOM}, indicating that the critical clusters may contain 4-5 HOM molecules, based on the classical homogeneous nucleation theory (Kashchiev, 1982), although there is a caveat that this assumption may not be accurate for atmospherically relevant particles (Ehrhart & Curtius, 2013; Kupiainen et al., 2012; Malila et al., 2015). As expected, the *GR* also increased with increasing P_{HOM}.

Using these results as the baseline conditions (α-pinene 238 ppb and ozone 1.2 ppm), we added isoprene gradually with the R ratio increasing from 0, 0.05, 0.2, 0.5, 1, 2.5, 5.2, and 11.2 (Figure S3 in Supporting Information S1). When R increased from 0 to approximately 2, there was a continuous reduction of particle number concentrations in all sizes, but after $R > 2$, particle concentrations increased. Nucleation rates also show a similar trend with R (Figure 1). We conducted the experiments under the same conditions for 6 days and they all showed the consistent trend as discussed here.

When comparing this trend with the OH and HO_2 concentrations calculated from the box model (Figure S4 in Supporting Information S1), it became clear that the turning point (R of ~2) is the condition where more than 90% of OH was scavenged by isoprene. As OH radicals were scavenged instantly by isoprene in the system and their maximum concentrations decreased with increasing R values, whereas HO_2 concentrations increased with R. Thus, while the suppression of NPF was related to the reduced OH (thus decreasing the monoterpene oxidation products) consistent with (McFiggans et al., 2019; Wang et al., 2021), but HO_2 also reacted with RO_2 radicals which prevented the formation of dimers (as opposed to $RO_2 + RO_2$ reactions). This analysis is further examined using the HOMs chemical composition measurements as discussed below.

During α-pinene and/or isoprene oxidation reactions, we identified the elemental composition of ~1,600 ion peaks. Tables S2 and S3 in Supporting Information S1 include 20 top HOMs signals for each experimental condition in the gas- and particle-phase, respectively. The general observation is as the following: regardless R values, the highest concentration of HOMs was in the range of C5–C10, with the components $C_9H_{14}O_4$ and $C_5H_{10}O_3$ having the highest concentrations in the gas phase, and a larger amount of C20 dimers present in the particle phase.

The mass defect plots clearly show the autoxidation production of HOMs (Figure 2). A large range of oxygen atoms, for example, in $C_{10}H_{16}O_x$ (x from 3 to 8) indicate that these highly oxygenated species indeed form from autoxidation reactions. The general pattern of mass defect plots of the gas- and aerosol-phase HOMs are strikingly similar, indicating that the gas-to-particle conversion process was dominant, and possible heterogenous reactions (such as oligomerization) were negligible within such a short reaction time (<200 s) in our experiments. Previous CLOUD studies have also shown similar elemental composition of HOMs in the gas- and aerosol-phase from the α-pinene/ozone or α-pinene/isoprene mixed systems (Caudillo et al., 2021; Q. Ye et al., 2019). In the pure α-pinene/ozone system, oxygenated C10 HOMs dominated the gas-phase spectra. However, even in the pure α-pinene system, there were abundant C5 and C15 HOMs, likely due to decomposition or fragmentation of C10 or C20 HOMs. C5 and C15 HOMs were also observed from the pure α-pinene/ozone system with the nitrate-CIMS by (Caudillo et al., 2021; Simon et al., 2020). The abundance of peaks seen above m/z 300 shows that particles formed in this pure α-pinene/ozone system contained a wide range of C20 HOMs. This is consistent with the formation of highly oxygenated, low volatility dimers that characterize monoterpene particle

10.1029/2023GL103545

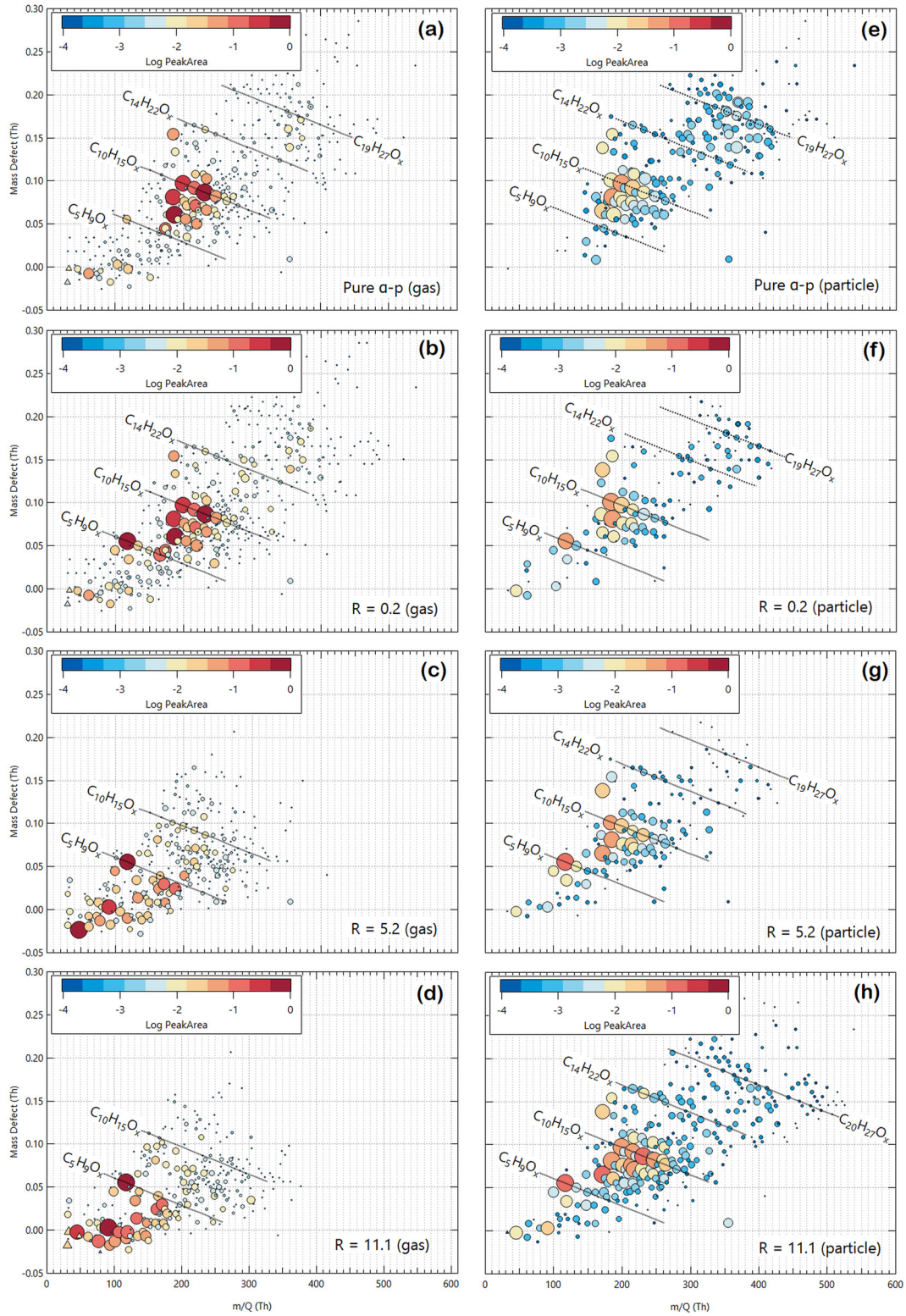

Figure 2. Mass defect plots for (a–d) gas- and (e–h) aerosol-phase highly oxygenated organic molecules measured simultaneously with the iodide high-resolution time-of-flight chemical ionization mass spectrometer. Experiments were conducted with (a, e) pure α-pinene, (b, f) $R = 0.2$ where a suppression of new particle formation (NPF) took place, and (c, g) $R = 5.2$ and (d, h) $R = 11.1$ where an enhancement of NPF took place. Color (in Log scale) and bubble size (in linear scale) indicate peak intensity.

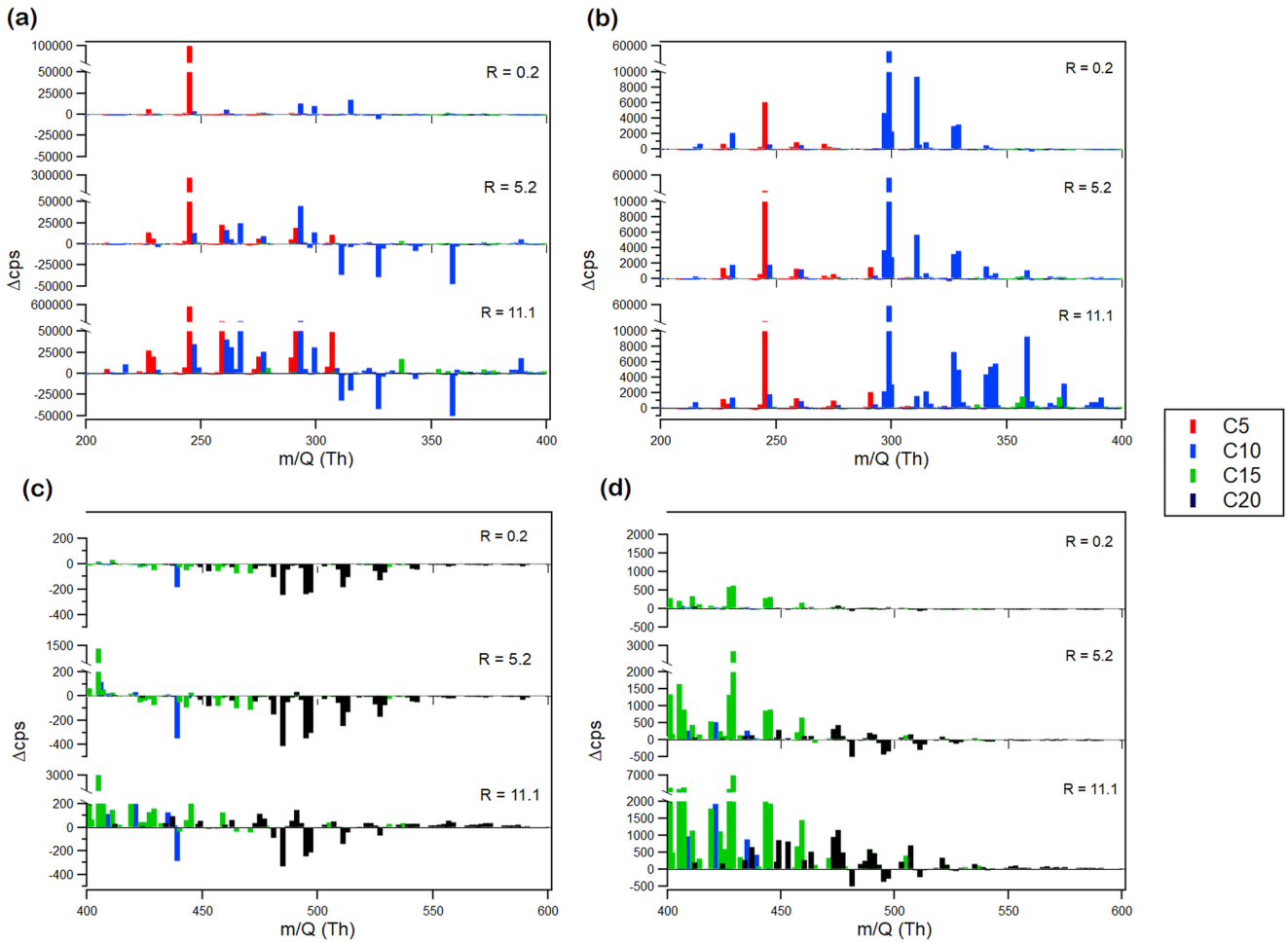

Figure 3. Stick plots showing differences in ion signal in the mass spectra taken at varying R values compared to the pure α-pinene spectra in the (a, c) gas and (b, d) particle phase. Negative peaks indicate stronger peaks in pure α-pinene spectrum, while positive peaks indicate stronger peaks in isoprene-containing spectra. Colors indicate highly oxygenated organic molecules classes based on the number of carbon atoms. Note that y-axes are split to maintain a consistent scale while still emphasizing the magnitude of the tallest peaks on each spectrum.

formation. As isoprene was added at low R values, signals for these C20 compounds weakened in both the gas- and particle-phase, consistent with the product suppression effects observed in previous studies (Heinritzi et al., 2020; McFiggans et al., 2019; Wang et al., 2021). Upon further increases in R, gas-phase C20 HOMs were suppressed, yet these signals were still significant in the particle-phase spectra. Thus, C20 HOMs that form under these high-isoprene conditions tended to partition very efficiently into particles. The C15 HOMs enhancement was also observed as R increased, but C15 compounds with higher masses were not detected in the particle phase outside of the highest isoprene concentrations. This suggests that in the presence of high concentrations of isoprene, it is not only favorable for C15 monoterpene/isoprene dimers to form, but there is an additional tendency for those C15 to have higher volatilities.

Figure 3 shows the relative changes in ion peaks in the mixed system as compared to the pure α-pinene oxidation system. Clearly, with the addition of isoprene, in both gas- and aerosol-phases, C5 and C15 HOMs were enhanced while C20 HOMs decreased. The increase in C5 and C15 concurrent with a decrease in C20 is evidence for both product scavenging, in which C15 compounds favorably form over C20 compounds, and $RO_2 + HO_2$ termination reactions, which suppress C20 while increasing monomer signals. When particle formation rates were suppressed at lower R values, there was a decrease for all C20 signals in the particle phase. However, C20 HOMs below m/z 500 were enhanced at higher R values. At $R = 5.2$, these lower mass C20 HOMs tended not to partition into the particle phase. At $R = 11.1$, these same C20 HOMs were detected in the particle phase, indicating that when a sufficient amount of isoprene oxidation products is available, lower mass (thus likely higher volatility) C20

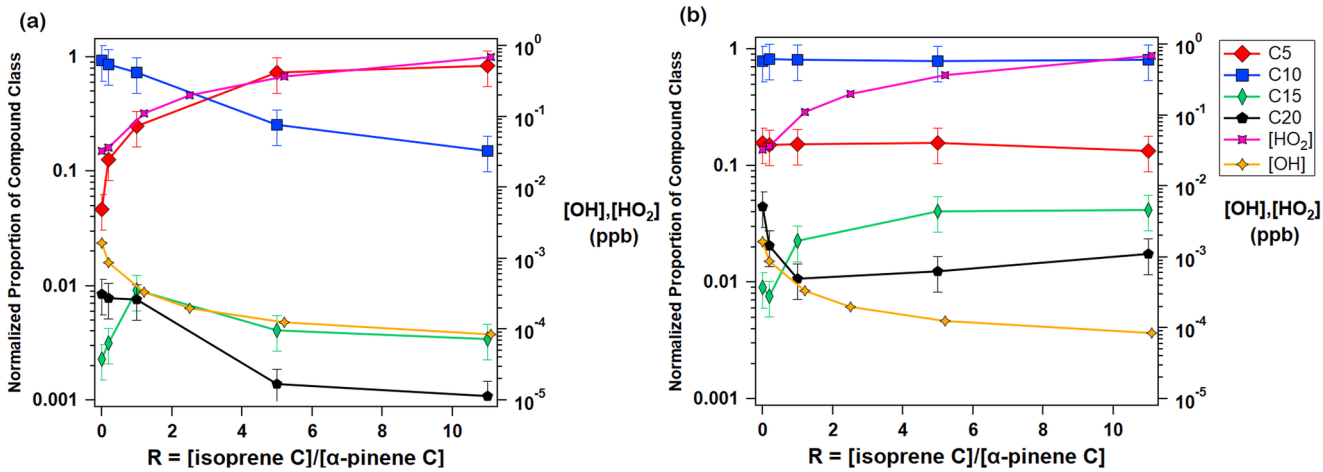

Figure 4. The normalized highly oxygenated organic molecules in the (a) gas-phase and (b) aerosol-phase for C5, C10, C15, and C20 groups and the box model-calculated OH and HO_2 concentrations are shown for different *R* conditions.

compounds are present in the particle phase. This may be due to the abundance of isoprene and ozone leading to rapid formation of isoprene oxidation products, which can react by RO_2-RO_2 reactions in to C20 compounds that tend to be less oxidized than those formed by monoterpene dimerization reactions. The abundant availability of these compounds at high values of *R* could result in more favorability for these compounds to partition into the particle phase. These trends indicate that within a certain class of HOMs (e.g., when simply grouped as C5, C10, C15, or C20), there exists a large range of volatilities that cannot be easily predicted from the elemental composition (or chemical formula) alone. Indeed, individual thermograms grouped by the HOM classes measured during this experiment showed a broad range of desorption temperature (Figure S5 in Supporting Information S1), indicating that conclusions of HOM volatility in this system demand a more granular analysis. Figure S5 in Supporting Information S1 shows the average thermogram profiles of HOMs for C5 (C5 only), C10 (C6–10), C15 (C11–15), and C20 (C16–20) groups. C5, C10, and C15 had a similar T_{max} ~70°C, corresponding to LogC* of approximately −3. On the other hand, C20 had a broader range of T_{max} between ~50 and 120°C approximately, corresponding to Log C* roughly between ~−1 and −7 and hence falling into the low volatility compounds and extremely low volatility compounds groups at room temperature (C. Ye et al., 2021; Ylisirniö et al., 2021). Thermograms of C10 compounds measured by (Caudillo et al., 2022) also showed a nearly 100°C range in desorption temperatures among compounds even with similar oxidation states, for example. Thus, the broad ranges of these thermograms indicate that a simple grouping of HOMs by the carbon number is insufficient to account for volatility differences in the particle phase. This is because even with the same chemical formula, there are different isomers that can have different oxidation status, and chemical functional groups can dictate the volatility of an organic compound more greatly compared to the number of carbon atoms.

A comparison of HOMs with OH and HO_2 concentrations reveals an interesting interplay between HO_x and isoprene (Figure 4). The box model was incorporated with the Master Chemical Mechanism (MCM) v.3.3.1 (Jenkin et al., 2015). Figure 4 shows the normalized ion intensities of C5, C10, C15–C20 HOMs in the gas- and aerosol-phase as a function of *R*. While OH decreased with increasing *R* values, HO_2 increased with *R*, as discussed above. As expected, HO_2 and C5 also showed very similar trends with varying *R* values, as they form from similar reaction pathways involving isoprene autoxidation reactions (Bates & Jacob, 2019). C10 HOMs decreased with the decreasing OH, indicating a significant portion of C10 HOMs in our experimental system were formed from the OH oxidation of α-pinene as well as ozonolysis. Additionally, the decrease in C10 is due to the presence of C5 RO_2 with increasing isoprene in the system, leading to C15-forming $RO_2 + RO_2$ reactions. Thus, the low *R* region (<~2) can be considered as dual oxidation regime where OH oxidation plays a dominant role in the formation of HOMs from monoterpenes, whereas as high *R* region (>~2) can be considered as the mostly ozone-oxidation regime with minimal OH concentrations.

At the low *R* region (<~2), the proportion of C15 present in both the gas- and particle-phase becomes dominant over C20 as C5 increases, which can be attributed to the product scavenging effects of C5 on C20 dimers. This is the region where NPF suppression was observed. In the gas-phase, we saw a significant decrease at low *R* in

C10 that was not present in the particle-phase, indicating that the mechanism of C20 suppression was not only due to the decrease in C10 proportion, but can also be attributed to the addition of C5 compounds in the system. As R became larger than ~2, HO_2 increases with a concurrent decrease in gas phase C15 and C20, indicating that $HO_2 + RO_2$ reactions were suppressing the formation of dimers (C15 and 20). In the gas phase, HOMs were dominated by C5 and C10 (they together account for more than 99% of total HOMs). On the other hand, the fraction of C15 and C20 HOMs in the particle phase was 4–5 times higher than in the gas phase (less than 1%), due to the active gas-to-particle conversion processes of these HOMs. C5 and C10 contents were nearly the same across different R values, because they were abundant in the gas phase and readily sufficient for aerosol formation. At higher R conditions, $J_{1.8}$ was greatly enhanced by the increasing fraction of C15 and C20. This enhancement was also likely due to the increased partitioning of abundant higher mass C10 molecules in to the particle phase as isoprene increased. While Figure 4b shows the proportion of C10 in the particle phase does not change, Figure 3b clearly shows an increase in particle-phase C10 at higher masses. This indicates that in the presence of isoprene it is likely that isoprene-derived C5 monomer RO_2 radicals react with one another to form oxidized dimer C10 that then efficiently partition in to the particle phase.

Our analysis shows that the low R region (<~2; in our experimental conditions) represents primarily the OH oxidation regime in the presence of ozone, whereas the high R region (>~2) represents the ozone oxidation. Table S1 in Supporting Information S1 compares different oxidation regimes and R conditions used in the previous studies. Heinritzi et al. (2020) used both OH and ozone were present in their experiments, but their R values were mostly at a small range of R (<2) with only a few exceptions. Thus, their experimental conditions resemble the low R condition, where continuous suppression of NPF by isoprene takes place due to the production effects of C20, as discussed above (Figure 4). In (McFiggans et al., 2019), the R values went higher, but their experiments were made at high concentrations of OH, thus in terms of oxidation chemistry, their conditions still resemble the low R condition. Wang et al. (2021) used both the OH + ozone oxidation and ozone-only oxidation regime, where they observed both the suppression and enhancement of NPF, respectively, similarly to the present study. Our study further demonstrates that in addition to the product suppression effects, $HO_2 + RO_2$ reactions also play important roles in the suppression of dimers (C15 and C20) and in biogenic NPF processes. It is possible that in real forests, $HO_2 + RO_2$ reactions may be even more important than product suppression effects, for example, depending on the relative concentrations of HO_2 versus RO_2 and the different $RO_2 + RO_2$ (or $RO_2 + R'O_2$) reaction rate coefficients. In the real atmosphere, R varies depending on season and atmospheric condition. R values can be as high as >10 (Kanawade et al., 2011; S.-H. Lee et al., 2016, 2019). The tipping point where suppression of NPF by isoprene shifts to enhancement was ~2 in our experimental conditions. However, as shown in the above analysis, this threshold value is sensitively dependent on the oxidation regime and VOCs composition and concentrations, and thus cannot be simply molded into real atmospheric environments.

4. Conclusions

Our biogenic NPF experiments show that isoprene can suppress biogenic NPF where OH oxidation is dominant (e.g., at a low R); but when the ozone oxidation is dominant with minimal OH radicals (at a high R), isoprene can also enhance NPF. While our results agree with previous studies on product suppression effects by isoprene (Heinritzi et al., 2020; McFiggans et al., 2019; Wang et al., 2021), we also find the $HO_2 + RO_2$ reactions are important for the suppression of dimer formation (C15 and C20), as occurring in the real atmosphere (Wang et al., 2021). Specifically, at conditions favorable to the suppression of NPF by isoprene, particle chemical composition suggests $RO_2 + HO_2$ termination reactions play an important role in the observed lack of particles. As R increases, product suppression occurs, which reduces the proportion of dimers consisting of two monoterpene units (C20 dimers) in favor of isoprene-monoterpene dimers (C15 dimers). Our results highlight the important synergetic effects of isoprene and HO_x on biogenic NPF.

At present, there are strong discrepancies in the literature amongst biogenic NPF studies involving isoprene (Heinritzi et al., 2020; McFiggans et al., 2019; Wang et al., 2021), and our analysis shows that seemingly inconsistent chemical mechanisms and interpretations provided from these previous studies were due to different oxidation regimes and different R ranges used in their experiments. Our results, together with these previous studies, can explain the lack of NPF events observed in pristine Amazon rainforests. However, to simulate the atmospheric conditions of mixed deciduous forests in the United States with substantial influences of man-made air pollutants (e.g., SO_2 and ammonia), additional work using the multicomponent nucleation systems is required.

Data Availability Statement

The data is available at Zenodo (https://doi.org/10.5281/zenodo.7864401) The MCM v3.3.1 model is available at Jenkin et al. (2015).

Acknowledgments
This study was supported by National Science Foundation (2209722, 2117389, and 2107916). We thank Asadullah Shoaib, Maxwell Ernst, and Yue Zhao for their assistants on experiments and data analysis.

References

Bae, M. S., Schwab, J. J., Hogrefe, O., Frank, B. P., Lala, G. G., & Demerjian, K. L. (2010). Characteristics of size distributions at urban and rural locations in New York. *Atmospheric Chemistry and Physics*, *10*, 4521–4535. https://doi.org/10.5194/acp-10-4521-2010

Bates, K. H., & Jacob, D. J. (2019). A new model mechanism for atmospheric oxidation of isoprene: Global effects on oxidants, nitrogen oxides, organic products, and secondary organic aerosol. *Atmospheric Chemistry and Physics*, *19*(14), 9613–9640. https://doi.org/10.5194/acp-19-9613-2019

Bianchi, F., Kurtén, T., Riva, M., Mohr, C., Rissanen, M. P., Roldin, P., et al. (2019). Highly oxygenated organic molecules (HOM) from gas-phase autoxidation involving peroxy radicals: A key contributor to atmospheric aerosol. *Chemical Reviews*, *119*(6), 3472–3509. https://doi.org/10.1021/acs.chemrev.8b00395

Caudillo, L., Rörup, B., Heinritzi, M., Marie, G., Simon, M., Wagner, A. C., et al. (2021). Chemical composition of nanoparticles from α-pinene nucleation and the influence of isoprene and relative humidity at low temperature. *Atmospheric Chemistry and Physics*, *21*(22), 17099–17114. https://doi.org/10.5194/acp-21-17099-2021

Caudillo, L., Surdu, M., Lopez, B., Wang, M., Thoma, M., Bräkling, S., et al. (2022). An intercomparison study of four different techniques for measuring the chemical composition of nanoparticles. *Atmospheric Chemistry and Physics Discussions*, *2022*, 1–24. https://doi.org/10.5194/acp-2022-498

Di Carlo, P., Brune, W. H., Martinez, M., Harder, H., Lesher, R., Ren, X., et al. (2004). Missing OH reactivity in a forest: Evidence for unknown reactive biogenic VOCs. *Science*, *304*(5671), 722–725. https://doi.org/10.1126/science.1094392

Ehrhart, S., & Curtius, J. (2013). Influence of aerosol lifetime on the interpretation of nucleation experiments with respect to the first nucleation theorem. *Atmospheric Chemistry and Physics*, *13*(22), 11465–11471. https://doi.org/10.5194/acp-13-11465-2013

Finlayson-Pitts, B. J., & Pitts, J. N. (2000). *Chemistry of the upper and lower atmosphere: Theory, experiments, and applications*. Academic Press.

Frege, C., Ortega, I. K., Rissanen, M. P., Praplan, A. P., Steiner, G., Heinritzi, M., et al. (2018). Influence of temperature on the molecular composition of ions and charged clusters during pure biogenic nucleation. *Atmospheric Chemistry and Physics*, *18*(1), 65–79. https://doi.org/10.5194/acp-18-65-2018

Gordon, H., Kirkby, J., Baltensperger, U., Bianchi, F., Breitenlechner, M., Curtius, J., et al. (2017). Causes and importance of new particle formation in the present-day and preindustrial atmospheres. *Journal of Geophysical Research: Atmospheres*, *122*(16), 8739–8760. https://doi.org/10.1002/2017jd026844

Guenther, A., Karl, T., Harley, P., Wiedinmyer, C., Palmer, P. I., & Geron, C. (2006). Estimates of global terrestrial isoprene emissions using MEGAN (model of emissions of gases and aerosols from nature). *Atmospheric Chemistry and Physics*, *6*(11), 3181–3210. https://doi.org/10.5194/acp-6-3181-2006

Hallar, A. G., Petersen, R., McCubbin, I. B., Lowenthal, D. H., Lee, S. H., Andrews, E., & Yu, F. (2015). Climatology of new particle formation and corresponding precursors at Storm Peak Laboratory. *Aerosol and Air Quality Research*, *10*. https://doi.org/10.4209/aaqr.2015.4205.0341

Heinritzi, M., Dada, L., Simon, M., Stolzenburg, D., Wagner, A. C., Fischer, L., et al. (2020). Molecular understanding of the suppression of new-particle formation by isoprene. *Atmospheric Chemistry and Physics*, *20*, 11809–11821. https://doi.org/10.5194/acp-2020-51

Hofzumahaus, A., Rohrer, F., Lu, K., Bohn, B., Brauers, T., Chang, C. C., et al. (2009). Amplified trace gas removal in the troposphere. *Science*, *324*(5935), 1702–1704. https://doi.org/10.1126/science.1164566

Iyer, S., Rissanen, M. P., Valiev, R., Barua, S., Krechmer, J. E., Thornton, J., et al. (2021). Molecular mechanism for rapid autoxidation in α-pinene ozonolysis. *Nature Communications*, *12*(1), 878. https://doi.org/10.1038/s41467-021-21172-w

Jenkin, M. E., Young, J. C., & Rickard, A. R. (2015). The MCM v3.3.1 degradation scheme for isoprene. *Atmospheric Chemistry and Physics*, *15*(20), 11433–11459. https://doi.org/10.5194/acp-15-11433-2015

Kanawade, V. P., Jobson, B. T., Guenther, A. B., Erupe, M. E., Pressley, S. N., Tripathi, S. N., & Lee, S. H. (2011). Isoprene suppression of new particle formation in a mixed deciduous forest. *Atmospheric Chemistry and Physics*, *11*(12), 6013–6027. https://doi.org/10.5194/acp-11-6013-2011

Kashchiev, D. (1982). On the relation between nucleation work, nucleus size, and nucleation rate. *Journal of Physical Chemistry*, *76*(10), 5098–5012. https://doi.org/10.1063/1.442808

Kerminen, V. M., Chen, X. M., Vakkari, V., Petaja, T., Kulmala, M., & Bianchi, F. (2018). Atmospheric new particle formation and growth: Review of field observations. *Environmental Research Letters*, *13*(10), 38. https://doi.org/10.1088/1748-9326/aadf3c

Kiendler-Scharr, A., Wildt, J., Dal Maso, M., Hohaus, T., Kleist, E., Mente, T. F., et al. (2009). New particle formation in forests inhibited by isoprene emissions. *Nature*, *461*(7262), 381–384. https://doi.org/10.1038/nature08292

Kupiainen, O., Ortega, I. K., Kurtén, T., & Vehkamäki, H. (2012). Amine substitution into sulfuric acid – Ammonia clusters. *Atmospheric Chemistry and Physics*, *12*(8), 3591–3599. https://doi.org/10.5194/acp-12-3591-2012

Lee, B. H., Lopez-Hilfiker, F. D., Mohr, C., Kurtén, T., Worsnop, D. R., & Thornton, J. A. (2014). An iodide-adduct high-resolution time-of-flight chemical-ionization mass spectrometer: Application to atmospheric inorganic and organic compounds. *Environmental Science & Technology*, *48*(11), 6309–6317. https://doi.org/10.1021/es500362a

Lee, S.-H., Gordon, H., Yu, H., Lehtipalo, K., Haley, R., Li, Y., & Zhang, R. (2019). New particle formation in the atmosphere: From molecular clusters to global climate. *Journal of Geophysical Research: Atmospheres*, *124*(13), 7098–7146. https://doi.org/10.1029/2018JD029356

Lee, S.-H., Uin, J., Guenther, A. B., Gouw, J. A., Yu, F., Nadykto, A. B., et al. (2016). Isoprene suppression of new particle formation: Potential mechanism and implications. *Journal of Geophysical Research*, *121*(24), 14621–14635. https://doi.org/10.1029/2016JD024844

Lehtipalo, K., Leppä, J., Kontkanen, J., Kangasluoma, J., Franchin, A., Wimnner, D., et al. (2014). Methods for determining particle size distribution and growth rates between 1 and 3 nm using the Particle Size Magnifier. *Boreal Environment Research*, *19*, 215–236.

Lelieveld, J., Butler, T. M., Crowley, J. N., Dillon, T. J., Fischer, H., Ganzeveld, L., et al. (2008). Atmospheric oxidation capacity sustained by a tropical forest. *Nature*, *452*(7188), 737–740. https://doi.org/10.1038/nature06870

Lopez-Hilfiker, F. D., Mohr, C., Ehn, M., Rubach, F., Kleist, E., Wildt, J., et al. (2014). A novel method for online analysis of gas and particle composition: Description and evaluation of a filter inlet for gases and AEROsols (FIGAERO). *Atmospheric Measurement Techniques*, *7*(4), 983–1001. https://doi.org/10.5194/amt-7-983-2014

Malila, J., McGraw, R., Laaksonen, A., & Lehtinen, K. E. J. (2015). Communication: Kinetics of scavenging of small, nucleating clusters: First nucleation theorem and sum rules. *The Journal of Chemical Physics*, *142*(1), 011102. https://doi.org/10.1063/1.4905213

Martinez, M., Harder, H., Kubistin, D., Rudolf, M., Bozem, H., Eerdekens, G., et al. (2010). Hydroxyl radicals in the tropical troposphere over the Suriname rainforest: Airborne measurements. *Atmospheric Chemistry and Physics*, *10*(8), 3759–3773. https://doi.org/10.5194/acp-10-3759-2010

McFiggans, G., Mentel, T. F., Wildt, J., Pullinen, I., Kang, S., Kleist, E., et al. (2019). Secondary organic aerosol reduced by mixture of atmospheric vapours. *Nature*, *565*(7741), 587–593. https://doi.org/10.1038/s41586-018-0871-y

Paulot, F., Crounse, J. D., Kiaergaard, J. G., Kurten, A., St. Clair, J. M., Seinfeld, J. H., & Wennberg, P. O. (2009). Unexpected epoxide formation in the gas-phase photooxidation of isoprene. *Science*, *325*(5941), 730–733. https://doi.org/10.1126/science.1172910

Peeters, J., Nguyen, T. L., & Vereecken, L. (2009). HO_x radical regeneration in the oxidation of isoprene. *Physical Chemistry Chemical Physics*, *11*(28), 5935–5939. https://doi.org/10.1039/b908511d

Pillai, P., Khlystov, A., Walker, J., & Aneja, V. (2013). Observation and analysis of particle nucleation at a forest site in Southeastern U.S. atmosphere. *Atmosphere*, *4*(2), 72–93. https://doi.org/10.3390/atmos4020072

Pöhlker, C., Wiedemann, K. T., Sinha, B., Shiraiwa, M., Gunthe, S. S., Smith, M., et al. (2012). Biogenic potassium salt particles as seeds for secondary organic aerosol in the Amazon. *Science*, *337*(6098), 1075–1078. https://doi.org/10.1126/science.1223264

Rissler, J. A., Vestin, A., Swietlicki, E., Fisch, G., Zhou, J., Artaxo, P., & Andrae, M. O. (2006). Size distribution and hygroscopic properties of aerosol particles from dry season biomass burning in Amazonia. *Atmospheric Chemistry and Physics*, *6*(2), 471–491. https://doi.org/10.5194/acp-6-471-2006

Riva, M., Heikkinen, L., Bell, D. M., Peräkylä, O., Zha, Q., Schallhart, S., et al. (2019). Chemical transformations in monoterpene-derived organic aerosol enhanced by inorganic composition. *npj Climate and Atmospheric Science*, *2*(1), 2. https://doi.org/10.1038/s41612-018-0058-0

Seinfeld, J. H., & Pandis, S. N. (2016). *Atmospheric chemistry and physics: From air pollution to climate change*. John Wiley and Sons, Inc.

Simon, M., Dada, L., Heinritzi, M., Scholz, W., Stolzenburg, D., Fischer, L., et al. (2020). Molecular understanding of new-particle formation from alpha-pinene between -50°C and 25°C. *Atmospheric Chemistry and Physics*, *20*, 65–79. https://doi.org/10.5194/acp-2019-1058

Tiszenkel, L., Stangl, C., Krasnomowitz, J., Ouyang, Q., Yu, H., Apsokardu, M. J., et al. (2019). Temperature effects on sulfuric acid aerosol nucleation and growth: Initial results from the TANGENT study. *Atmospheric Chemistry and Physics*, *19*(13), 8915–8929. https://doi.org/10.5194/acp-19-8915-2019

Tröstl, J., Chuang, W. K., Gordon, H., Heinritzi, M., Yan, C., Molteni, U., et al. (2016). The role of low-volatility organic compounds in initial particle growth in the atmosphere. *Nature*, *533*(7604), 527–531. https://doi.org/10.1038/nature18271

Vanhanen, J., Mikkila, J., Lehtipalo, K., Sipila, M., Manninen, H. E., Siivola, E., et al. (2011). Particle size magnifier for nano-CN detection. *Aerosol Science & Technology*, *45*(4), 533–542. https://doi.org/10.1080/02786826.2010.547889

Wang, Y., Zhao, Y., Li, Z., Li, C., Yan, N., & Xiao, H. (2021). Importance of hydroxyl radical chemistry in isoprene suppression of Particle Formation from α-pinene ozonolysis. *ACS Earth and Space Chemistry*, *5*(3), 487–499. https://doi.org/10.1021/acsearthspacechem.0c00294

Ye, C., Yuan, B., Lin, Y., Wang, Z., Hu, W., Li, T., et al. (2021). Chemical characterization of oxygenated organic compounds in the gas phase and particle phase using iodide CIMS with FIGAERO in urban air. *Atmospheric Chemistry and Physics*, *21*(11), 8455–8478. https://doi.org/10.5194/acp-21-8455-2021

Ye, Q., Wang, M., Hofbauer, V., Stolzenburg, D., Chen, D., Schervish, M., et al. (2019). Molecular composition and volatility of nucleated particles from α-pinene oxidation between −50°C and +25°C. *Environmental Science & Technology*, *53*(21), 12357–12365. https://doi.org/10.1021/acs.est.9b03265

Ylisirniö, A., Barreira, L. M. F., Pullinen, I., Buchholz, A., Jayne, J., Krechmer, J. E., et al. (2021). On the calibration of FIGAERO-ToF-CIMS: Importance and impact of calibrant delivery for the particle-phase calibration. *Atmospheric Measurement Techniques*, *14*(1), 355–367. https://doi.org/10.5194/amt-14-355-2021

You, Y., Kanawade, V. P., de Gouw, J. A., Guenther, A. B., Madronich, S., Sierra-Hernández, M. R., et al. (2014). Atmospheric amines and ammonia measured with a chemical ionization mass spectrometer (CIMS). *Atmospheric Chemistry and Physics*, *14*, 12181–12194. https://doi.org/10.5194/acpd-14-16411-2014

Yu, F., Luo, G., Pryor, S. C., Pillai, P. R., Lee, S. H., Ortega, J., et al. (2015). Spring and summer contrast in new particle formation over nine forest areas in North America. *Atmospheric Chemistry and Physics*, *15*, 13993–14003. https://doi.org/10.5194/acpd-15-21271-2015

Yu, H., & Lee, S.-H. (2012). Chemical ionisation mass spectrometry for the measurement of atmospheric amines. *Environmental Chemistry*, *9*(3), 190–201. https://doi.org/10.1071/en12020

Zhao, Y., Thornton, J. A., & Pye, H. O. T. (2018). Quantitative constraints on autoxidation and dimer formation from direct probing of monoterpene-derived peroxy radical chemistry. *Proceedings of the National Academy of Sciences of the United States of America*, *115*(48), 12142–12147. https://doi.org/10.1073/pnas.1812147115

References From the Supporting Information

Atkinson, R., Baulch, D. L., Cox, R. A., Crowley, J. N., Hampson, R. F., Hynes, R. G., et al. (2006). Evaluated kinetic and photochemical data for atmospheric chemistry: Volume II – Gas phase reactions of organic species. *Atmospheric Chemistry and Physics*, *6*(11), 3625–4055. https://doi.org/10.5194/acp-6-3625-2006

Dada, L., Lehtipalo, K., Kontkanen, J., Nieminen, T., Baalbaki, R., Ahonen, L., et al. (2020). Formation and growth of sub-3-nm aerosol particles in experimental chambers. *Nature Protocols*, *15*(3), 1013–1040. https://doi.org/10.1038/s41596-019-0274-z

Davidovits, P., Kolb, C. E., Williams, L. R., Jayne, J. T., & Worsnop, D. R. (2006). Mass accommodation and chemical reactions at gas–liquid interfaces. *Chemical Reviews*, *106*(4), 1323–1354. https://doi.org/10.1021/cr040366k

Donahue, N. M., Epstein, S. A., Pandis, S. N., & Robinson, A. L. (2011). A two-dimensional volatility basis set: 1. Organic-aerosol mixing thermodynamics. *Atmospheric Chemistry and Physics*, *11*(7), 3303–3318. https://doi.org/10.5194/acp-11-3303-2011

Erupe, M. E., Viggiano, A. A., & Lee, S. H. (2011). The effect of trimethylamine on atmospheric nucleation involving H_2SO_4. *Atmospheric Chemistry and Physics*, *11*(10), 4767–4775. https://doi.org/10.5194/acp-11-4767-2011

Kirkby, J., Duplissy, J., Sengupta, K., Frege, C., Gordon, H., Williamson, C., et al. (2016). Ion-induced nucleation of pure biogenic particles. *Nature*, *533*(7604), 521–526. https://doi.org/10.1038/nature17953

Tang, M. J., Shiraiwa, M., Pöschl, U., Cox, R. A., & Kalberer, M. (2015). Compilation and evaluation of gas phase diffusion coefficients of reactive trace gases in the atmosphere: Volume 2. Diffusivities of organic compounds, pressure-normalised mean free paths, and average Knudsen numbers for gas uptake calculations. *Atmospheric Chemistry and Physics*, *15*(10), 5585–5598. https://doi.org/10.5194/acp-15-5585-2015

Young, L. H., Benson, D. R., Rifkha, F., Pierce, J. R., Junninen, H., Kulmala, M., & Lee, S. H. (2008). Laboratory studies of sulfuric acid and water binary homogeneous nucleation: Evaluation of laboratory setup and preliminary results. *Atmospheric Chemistry and Physics*, *8*, 1–20.

Yu, H., McGraw, R., & Lee, S. H. (2012). Effects of amines on formation of sub-3 nm particles and their subsequent growth. *Geophysical Research Letters*, *39*(2), L02807. https://doi.org/10.1029/2011gl050099